Glypican-3-targeted Macrophages Delivering Drug-loaded Exosomes Offer Efficient Cytotherapy in Mouse Models of Solid Tumours

Jinhu Liu[1], Huajun Zhao[1], Tong Gao[1], Xinyan Huang[1], Shujun Liu[1], Meichen Liu[1], Weiwei Mu[1], Shuang Liang[1], Shunli Fu[1], Shijun Yuan[1], Qinglin Yang[1], Panpan Gu[1], Nan Li[1], Qingping Ma[1], Jie Liu[1], Xinke Zhang[1], Na Zhang[1]*, Yongjun Liu[1]*

[1]NMPA Key Laboratory for Technology Research and Evaluation of Drug Products and Key Laboratory of Chemical Biology (Ministry of Education), Department of Pharmaceutics, School of Pharmaceutical Sciences, Cheeloo College of Medicine, Shandong University, 44 Wenhuaxi Road, Jinan, Shandong Province 250012, China

*Corresponding author.

E-mail: liuyongjun@sdu.edu.cn (Yongjun Liu); zhangnancy9@sdu.edu.cn (Na Zhang)

Table of contents

RILO@MG.

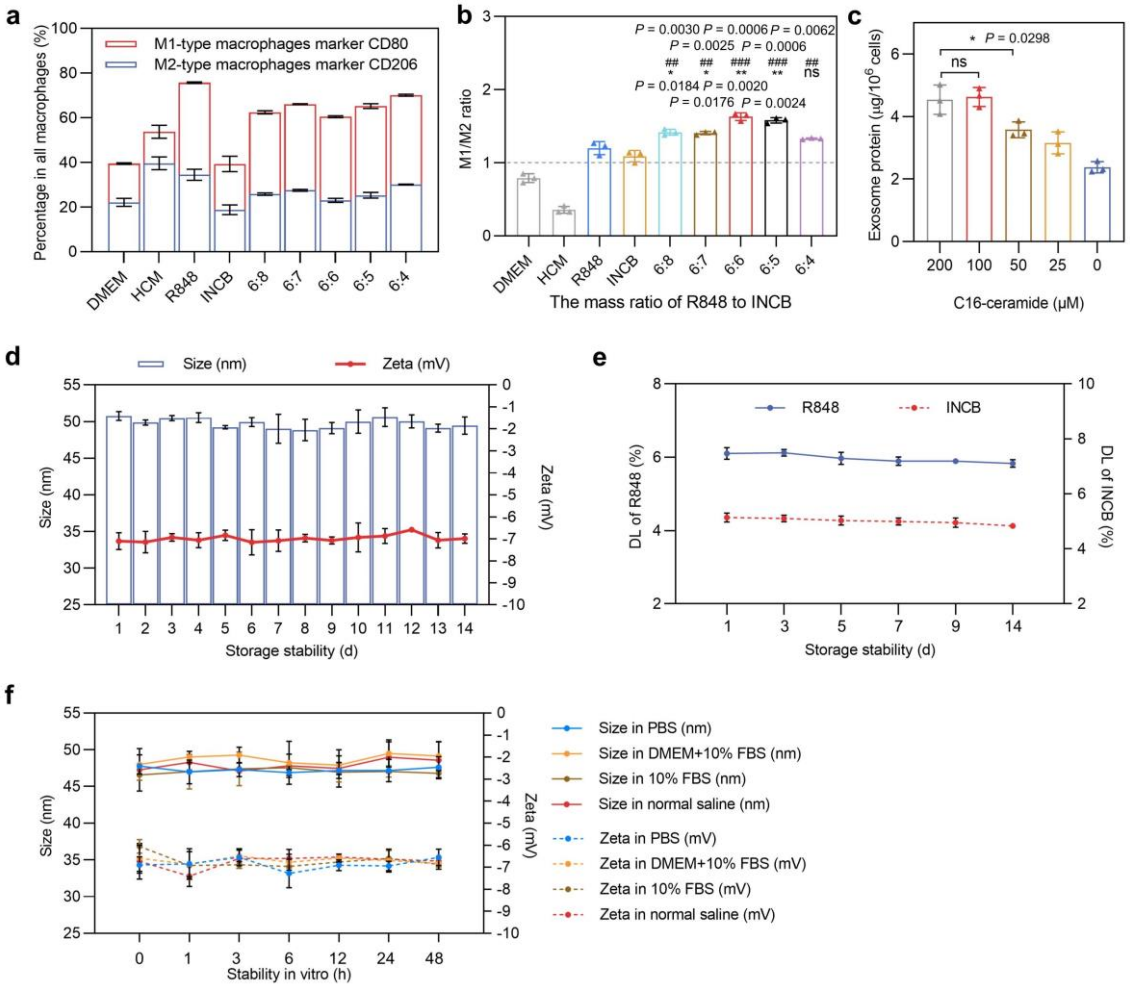

Supplementary Fig. 1. The prescription screens and stability of RILO. a, b, Effect of different mass ratio of R848 and INCB on TAM polarization. The percentage of M1-type macrophages marker CD80 and M2-type macrophages marker CD206 after incubated TAM^{RAW} with different mass ratios of R848 and INCB for 24 h in vitro (**a**). The ratio of M1-type macrophages to M2-type macrophages after incubation of TAM^{RAW} with different mass ratios of R848 and INCB for 24 h in vitro (**b**). TAM^{RAW} were generated by culturing RAW264.7 cells in HCM for 24 h. **P* and $^{\#}P$ indicate statistical significance compared to the R848 or INCB group, respectively. **c,** Effect of C16-ceramide concentration on released exosomes. After M1-type $macrophages^{RAW}$ were treated with various concentrations of C16-ceramide, released exosomes in 24 h were quantified. **d-f,** The stability of RILO under storage or physiological conditions. The changes of size and zeta potential of freshly prepared RILO with time after storage at 4 °C (**d**). The DL changes of R848 or INCB of freshly prepared RILO with time after storage at 4 °C (**e**). The size and zeta potential of RILO after incubation at PBS, DMEM contained 10% FBS, 10% FBS and normal saline at different time points (**f**). Data are expressed as the mean ± SD with 3 biologically independent experiments. Two-tailed Student's *t* test (**b**) or one-way ANOVA with Tukey's multiple comparisons test (**c**) was carried out for statistical analysis. **P* < 0.05; ***P* < 0.01; ****P* < 0.001; ns, no significance.

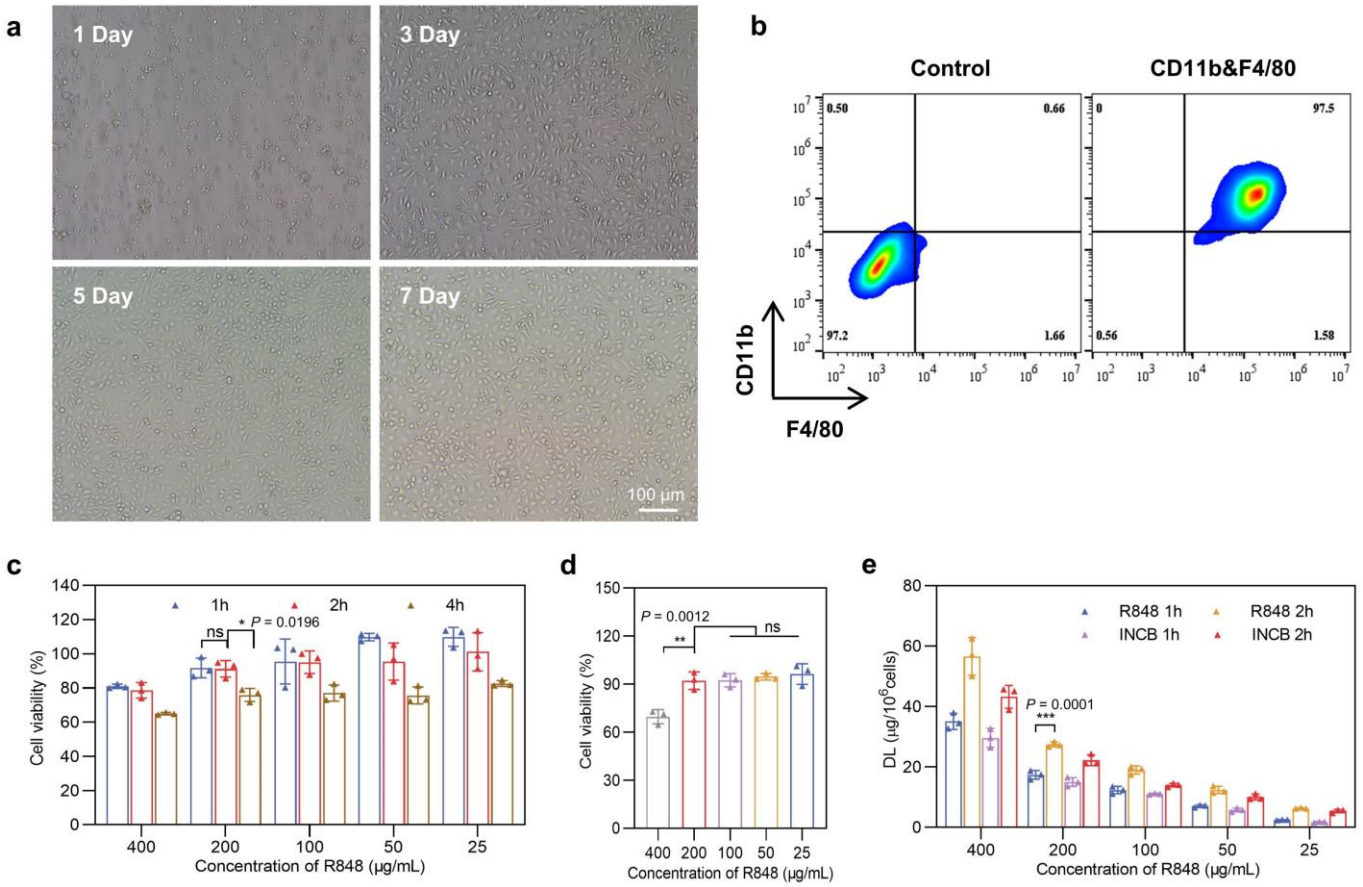

Supplementary Fig. 2. The optimizations of incubation concentration and time on cell viability and DL. a, b, Identification experiment of BMDMs (*n* = 3 biologically independent experiments). Representative images of morphological identification (**a**). On day 1, the myeloid cells isolated from bone marrow were round and suspended in the medium. On day 3, the adherent cells were macrophages with round or fusiform after removing the unadherent cells. On day 7, the macrophages were collected for further use. Scale bar, 100 μm. Representative flow cytometric analysis images of BMDMs formation on day 7 (**b**). Mature BMDMs were defined as $CD11b^{+}F4/80^{+}$ subpopulation (upper right) with the purity displayed as percentage higher than 95%. **c,** In vitro cell viability of different incubation concentrations and time of RILO on M1-type $macrophages^{RAW}$ (*n* = 3 biologically independent experiments). **d,** In vitro cell viability of different incubation concentrations of RILO on M1-type $macrophages^{BMDM}$ for incubating 2 h (*n* = 3 biologically independent experiments). **e,** The DL of different incubation concentrations and time of RILO on M1-type $macrophages^{RAW}$ (*n* = 3 biologically independent experiments). All data are shown as the mean ± SD. Two-tailed Student's *t* test (**e**) or one-way ANOVA with Tukey's multiple comparisons test (**c, d**) was carried out for statistical analysis. **P* < 0.05; ***P* < 0.01; ****P* < 0.001; ns, no significance.

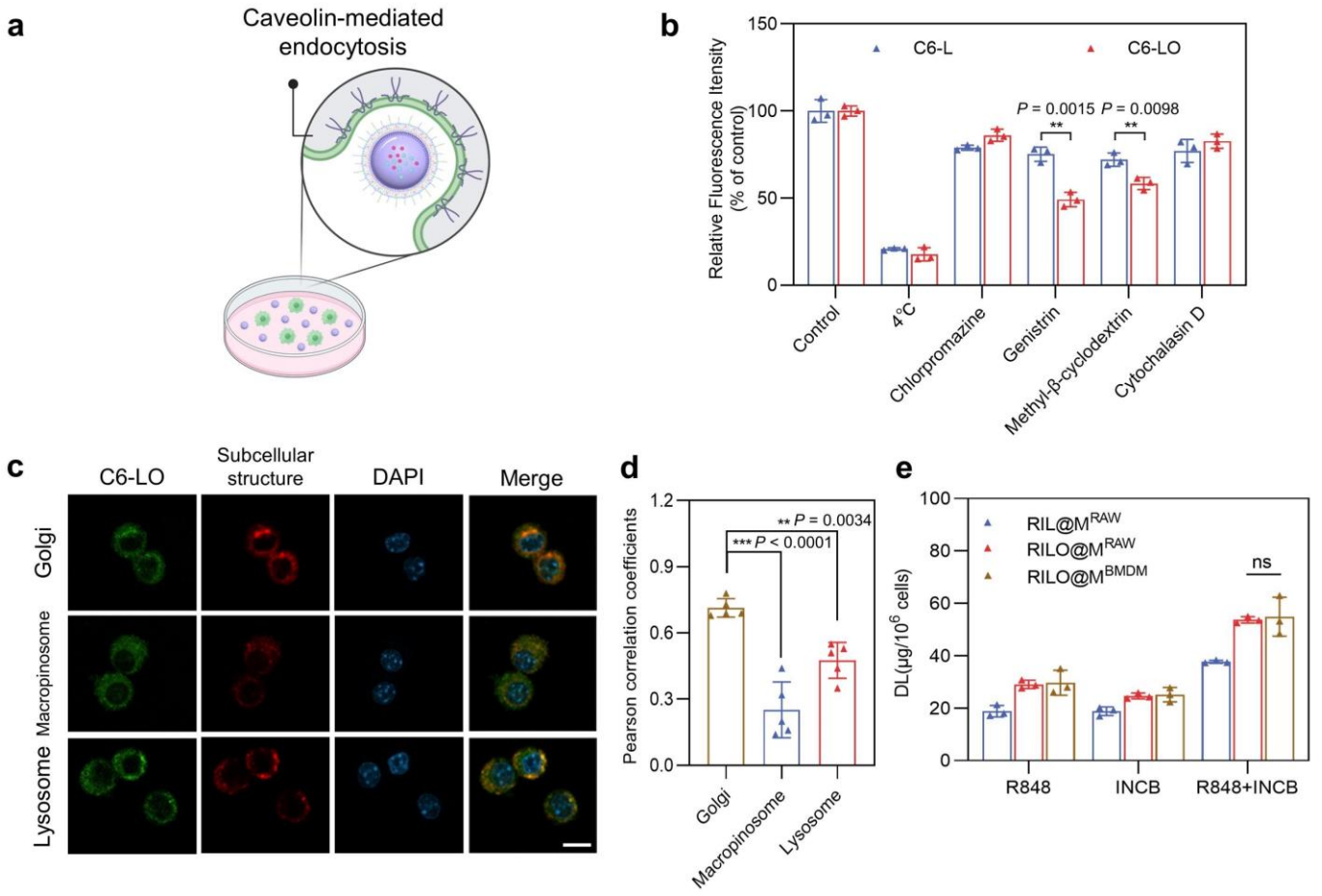

Supplementary Fig. 3. Endocytic pathways and the subsequent intracellular trafficking of C6-LO in M1-type macrophages. a, Schematic illustration of the uptake of RILO by M1-type macrophages via caveolin-mediated endocytosis. **b,** Effect of inhibitors on the uptake of C6-L or C6-LO by M1-type macrophages. Flow cytometry analysis of the inhibitor effect on the uptake of C6-L or C6-LO by M1-type macrophages in terms of C6 intensity (*n* = 3 biologically independent experiments). M1-type macrophages were pretreated with each inhibitor for 0.5 h, and then incubated with C6-L or C6-LO (200 ng/mL) for 2 h. C6 intensity was examined by flow cytometry. **c, d,** Intracellular trafficking of C6-LO in M1-type macrophages. Representative confocal images of colocalization of C6-LO and golgi tracker red, macropinosome tracker (70kd RhoB-Dextran) or lysosome tracker red after 6 h cultured with M1-type macrophages^{RAW} (**c**). Scale bar, 10 μm. Pearson correlation coefficients (**d**) of C6-LO (green) and subcellular structure tracker (red) fluorescence calculated using Image J software by pixel intensity (*n* = 5 biologically independent experiments). **e,** The DL of RIL@M^{RAW}, RILO@M^{RAW} and RILO@M^{BMDM}. RIL@M^{RAW}, RILO@M^{RAW} or RILO@M^{BMDM} was prepared by incubating RAW264.7 cells or BMDMs with RIL or RILO at 200 μg/mL (quantified by R848) at 37 °C for 2 h (*n* = 3 biologically independent experiments). All data are shown as the mean ± SD and were analysed by two-tailed Student's t test (**b, e**) or one-way ANOVA with Tukey's multiple comparisons test (**d**). $^{**}P < 0.01$; $^{***}P < 0.001$; ns, no significance.

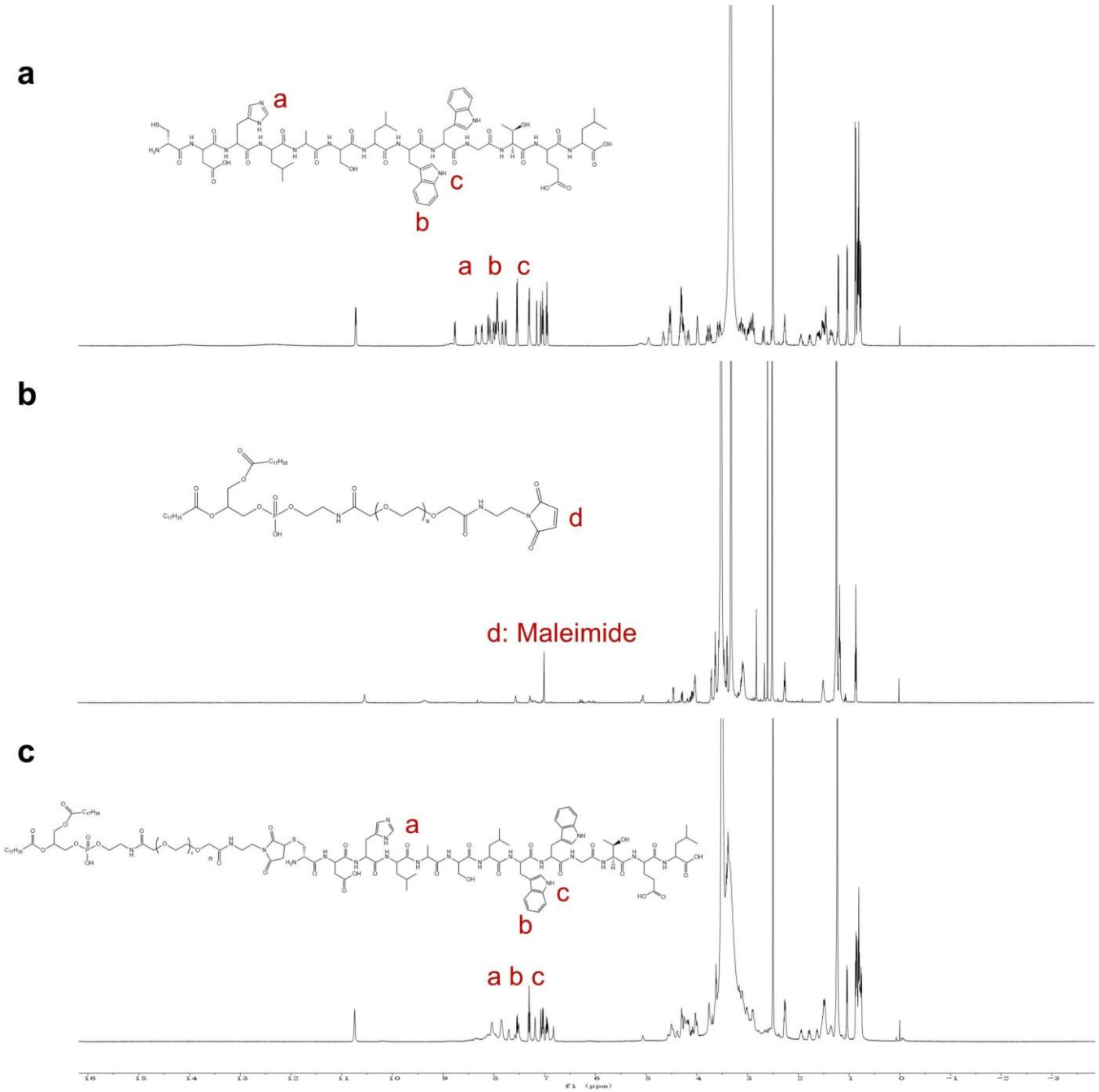

Supplementary Fig. 4. Synthesis and characterization of GTP, DSPE-PEG$_{5k}$ and DSPE-PEG$_{5k}$-GTP. a, The ^{1}H-NMR spectrum of GTP-SH. **b,** The ^{1}H-NMR spectrum of DSPE-PEG$_{5k}$-Mal. **c,** The ^{1}H-NMR spectrum of DSPE-PEG$_{5k}$-GTP. GPC3-targeting material DSPE-PEG$_{5k}$-GTP was synthesized through the reaction of maleimide in DSPE-PEG$_{5k}$-Mal with the sulfhydryl group of GTP-SH. The characteristic peak d of maleimide at 7.00 ppm in DSPE-PEG$_{5k}$-GTP disappeared, while GTP-SH related characteristic peaks a, b and c from 6.83 ppm to 8.36 ppm appeared, indicating the successful synthesis of DSPE-PEG$_{5k}$-GTP. The grafting rate of GTP was 19.78±0.10% in DSPE-PEG$_{5k}$-GTP determined by HPLC.

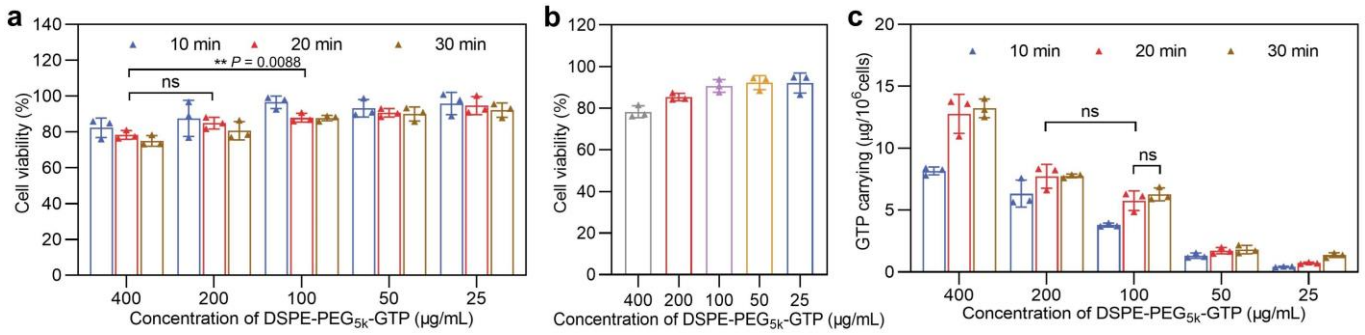

Supplementary Fig. 5. The optimizations of incubation concentrations and time on cell viability and GTP carrying. a, In vitro cell viability of different incubation concentrations and time of DSPE-PEG$_{5k}$-GTP on RILO@M^{RAW}. **b,** In vitro cell viability of different incubation concentrations of DSPE-PEG$_{5k}$-GTP on RILO@M^{BMDM} for incubating 20 min. **c,** The GTP carrying of different incubation concentrations and time of DSPE-PEG$_{5k}$-GTP on RILO@M^{RAW}. In addition, the GTP carrying of RILO@MG^{BMDM} was 6.67±0.64 μg/10^{6}cells at the optimal incubation concentration and time, which slightly higher than RILO@MG^{RAW} (5.76±0.79 μg/10^{6}cells). However, there was no significant difference between them, which were analysed by the two-tailed Student's *t*-test. Data are expressed as the mean ± SD with 3 biologically independent experiments. Two-way ANOVA with Tukey's multiple comparisons test (**a, c**) was carried out for statistical analysis. ***P* < 0.01; ns, no significance.

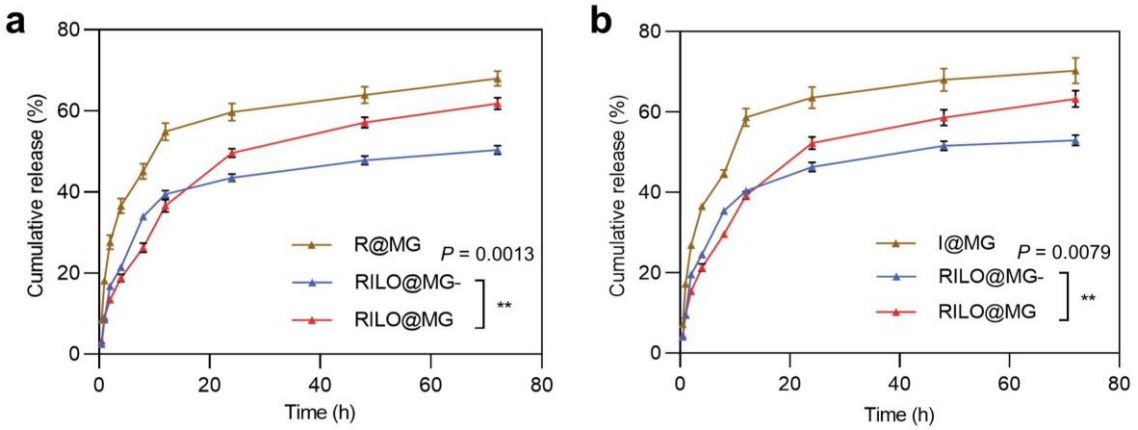

Supplementary Fig. 6. Release profiles of total drugs from RILO@MG. a, Release profiles during 72 h of total R848 from RILO@MG (*n* = 3 biologically independent experiments). **b,** Release profiles during 72 h of total INCB from RILO@MG (*n* = 3 biologically independent experiments). All data are shown as the mean ± SD and the data were analysed by two-way ANOVA with Tukey's multiple comparisons test. ***P* < 0.01.

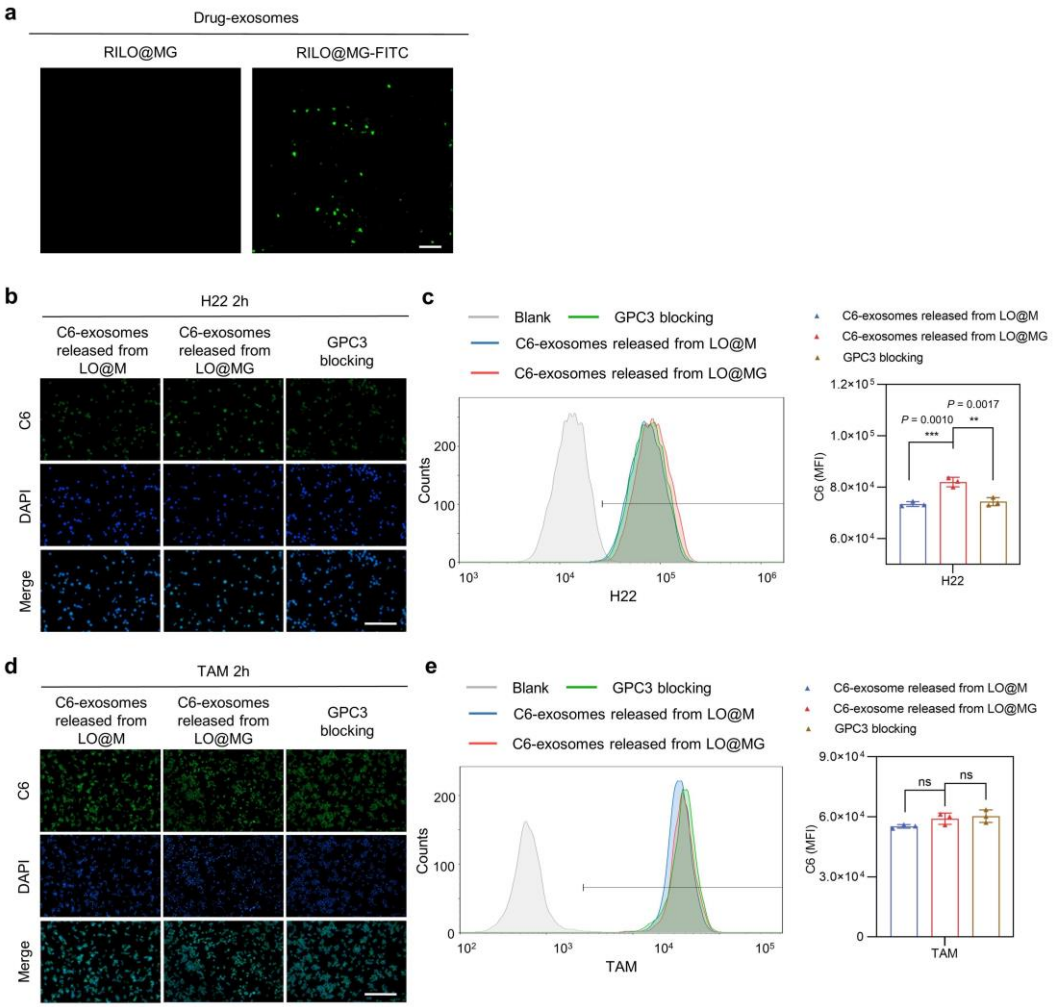

Supplementary Fig. 7. The uptake experiments of C6-exosomes released from different formulations. a, The ultra high resolution microscopy images of released exosomes (*n* = 3 biologically independent experiments). The RI-exosomes generated cumulatively at 48 h from RILO@MG and RILO@MG-FITC were separated and collected by serial centrifugation and ultracentrifugation. The RI-exosomes were imaged using a ultra high resolution microscope (DeltaVision OMX Flex, GE HealthCare, NJ, USA). **b, c,** The uptake experiments of C6-exosomes released from different formulations by H22 cells. C6-exosomes released cumulatively at 48 h from LO@M and LO@MG were separated and collected for these experiments. Fluorescence microscopy images (**b**) and flow cytometric analysis (**c**) of the uptake of C6-exosomes released from LO@M, C6-exosomes released from LO@MG and GPC3 blocking groups by H22 cells for 2 h in the same concentration (200 ng/mL) of C6 (*n* = 3 biologically independent experiments). **d, e,** The uptake experiments of C6-exosomes released from different formulations by TAM. C6-exosomes released cumulatively at 48 h from LO@M and LO@MG were separated and collected for these experiments. Fluorescence microscopy images (**a**) and flow cytometric analysis (**b**) of the uptake of C6-exosomes released from LO@M, C6-exosomes released from LO@MG and GPC3 blocking groups by TAMs for 2 h in the same concentration (200 ng/mL) of C6 (*n* = 3 biologically independent experiments). All data are shown as the mean ± SD and were analysed by one-way ANOVA with Tukey's multiple comparisons test. ***P* < 0.01; ****P* < 0.001; ns, no significance.

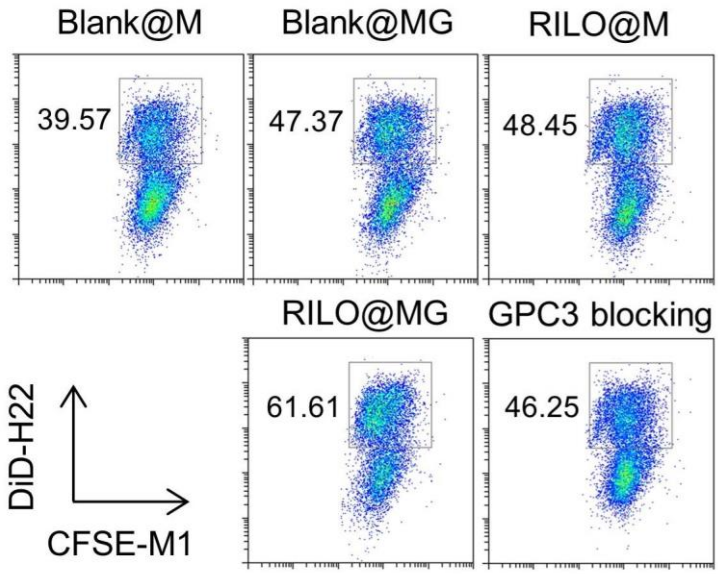

Supplementary Fig. 8. Effect of anchoring of GTP on phagocytosis. Representative flow cytometry plots related to Fig. 5c. DiD and CFSE were selected to label H22 cells and M1-type macrophages, respectively. The boxes within the plots showed the M1-type macrophages that phagocytized H22 cells (*n* = 3 biologically independent experiments).

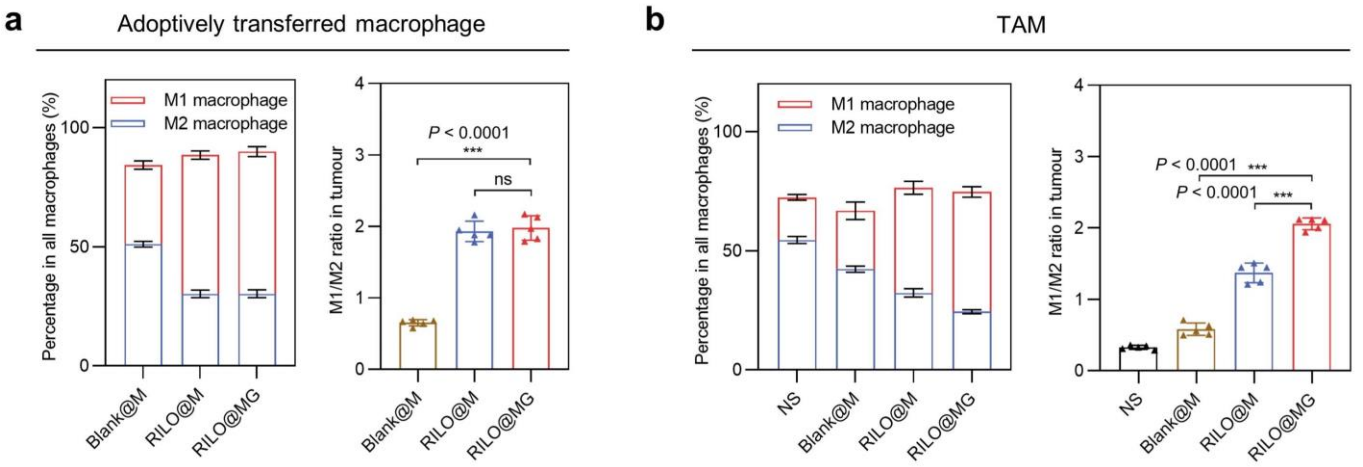

Supplementary Fig. 9. The phenotype analysis of adoptively transferred macrophage and TAM after injection. Mice inoculated with H22 cells were treated with adoptively transferred macrophage labeled with IVISense 680 fluorescent cell labeling dye. The intratumoural macrophage contained adoptively transferred macrophage and endogenous TAM, and the adoptively transferred macrophage could be distinguished by a flow cytometer. **a**, The phenotype analysis of adoptively transferred macrophage after i.v. administration with different formulations based on macrophages (n = 5 biologically independent animals). **b**, The phenotype analysis of endogenous TAM after injection of groups related to **a** (n = 5 biologically independent animals). All data are shown as the mean ± SD and were analysed by one-way ANOVA with Tukey's multiple comparisons test. ***P < 0.001; ns, no significance.

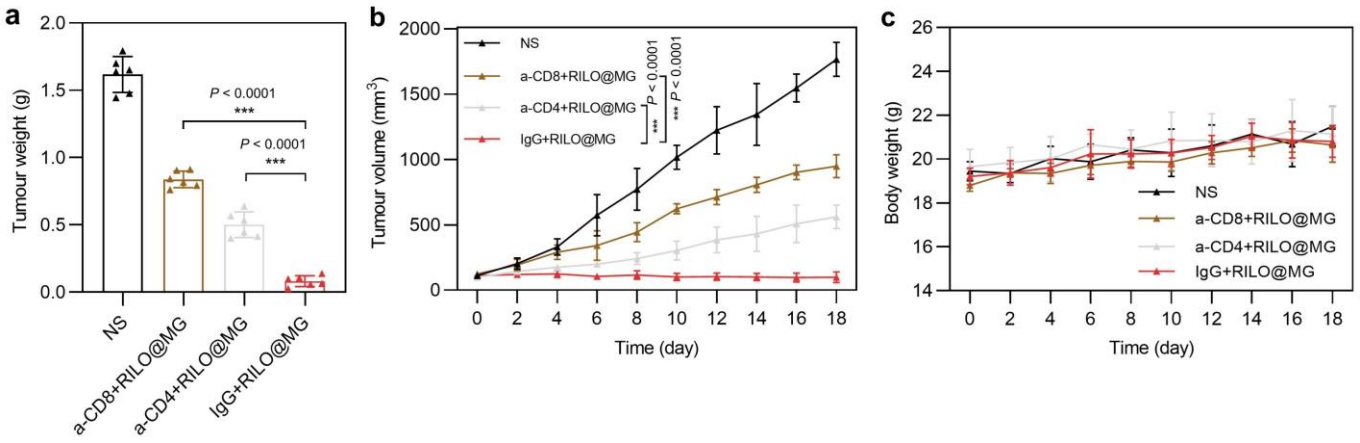

Supplementary Fig. 10. Tumour weights, average tumour growth curves and body weight changes over the course of treatment related to Fig. 5k-m. a, Tumour weights of H22 tumour-bearing mice (n = 6 biologically independent animals per group). **b**, Average tumour growth curves of H22 tumour-bearing mice (n = 6 biologically independent animals per group). **c,** body weight changes of H22 tumour-bearing mice (n = 6 biologically independent animals per group). All data are shown as the mean ± SD. One-way ANOVA with Tukey's multiple comparisons test (**a**) and two-way ANOVA with repeated measures (**b**) were carried out for statistical analysis. ***P < 0.001.

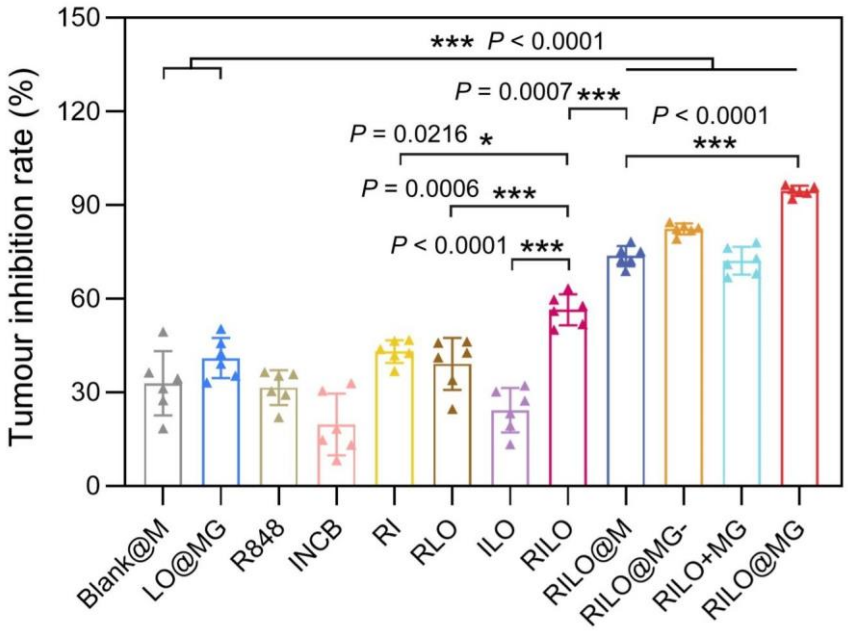

Supplementary Fig. 11. Tumour inhibition rate calculated based on Fig. 6d. All data are shown as the mean ± SD with *n* = 6 biologically independent animals. All data were analysed by one-way ANOVA with Tukey's multiple comparisons test. **P* < 0.05; ****P* < 0.001.

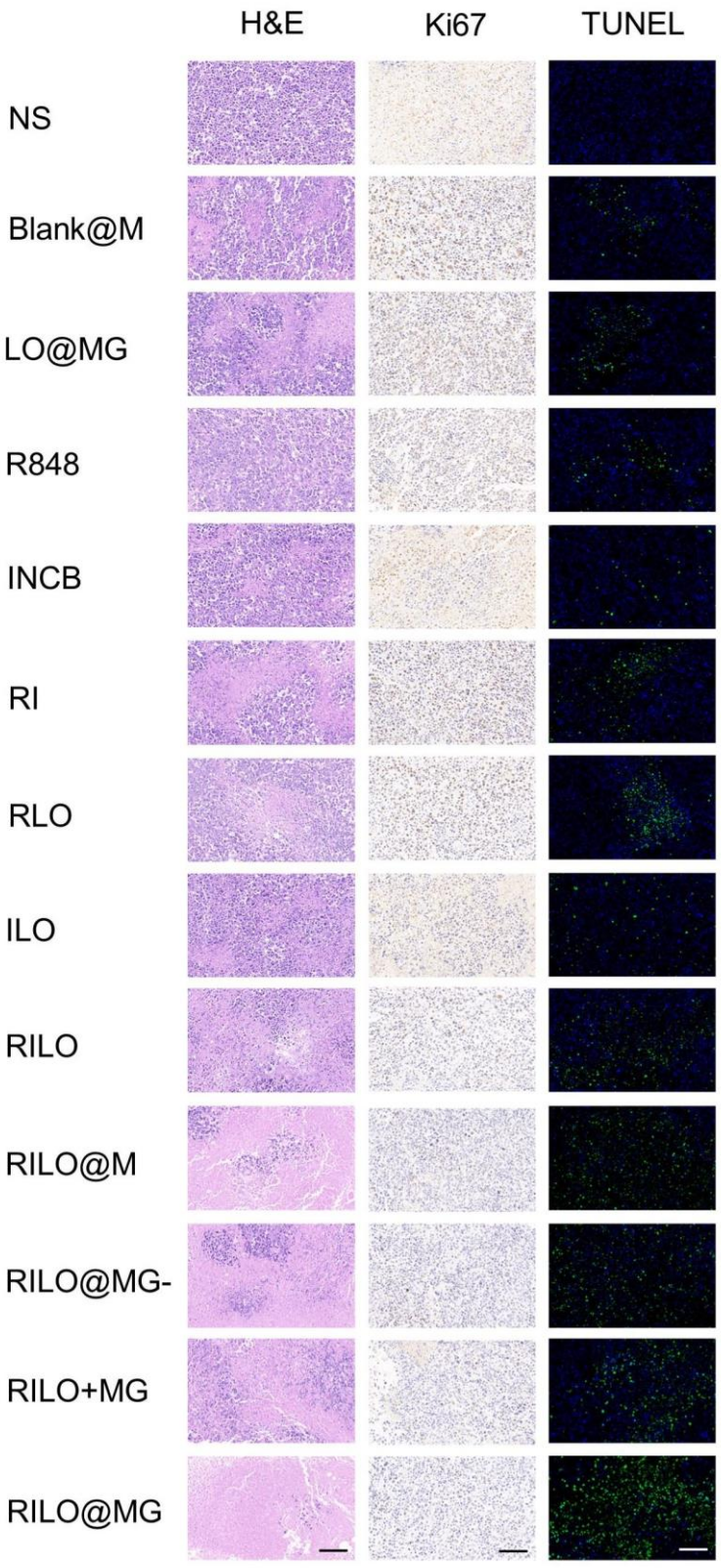

Supplementary Fig. 12. Representative images of tumour tissue sections related to Fig. 6a-f. Tumour tissues were obtained at the study endpoint. H&E, Ki67, and TUNEL staining were performed on tissue sections for pathological assessment (*n* = 3 biologically independent experiments). Scale bar = 100 μm.

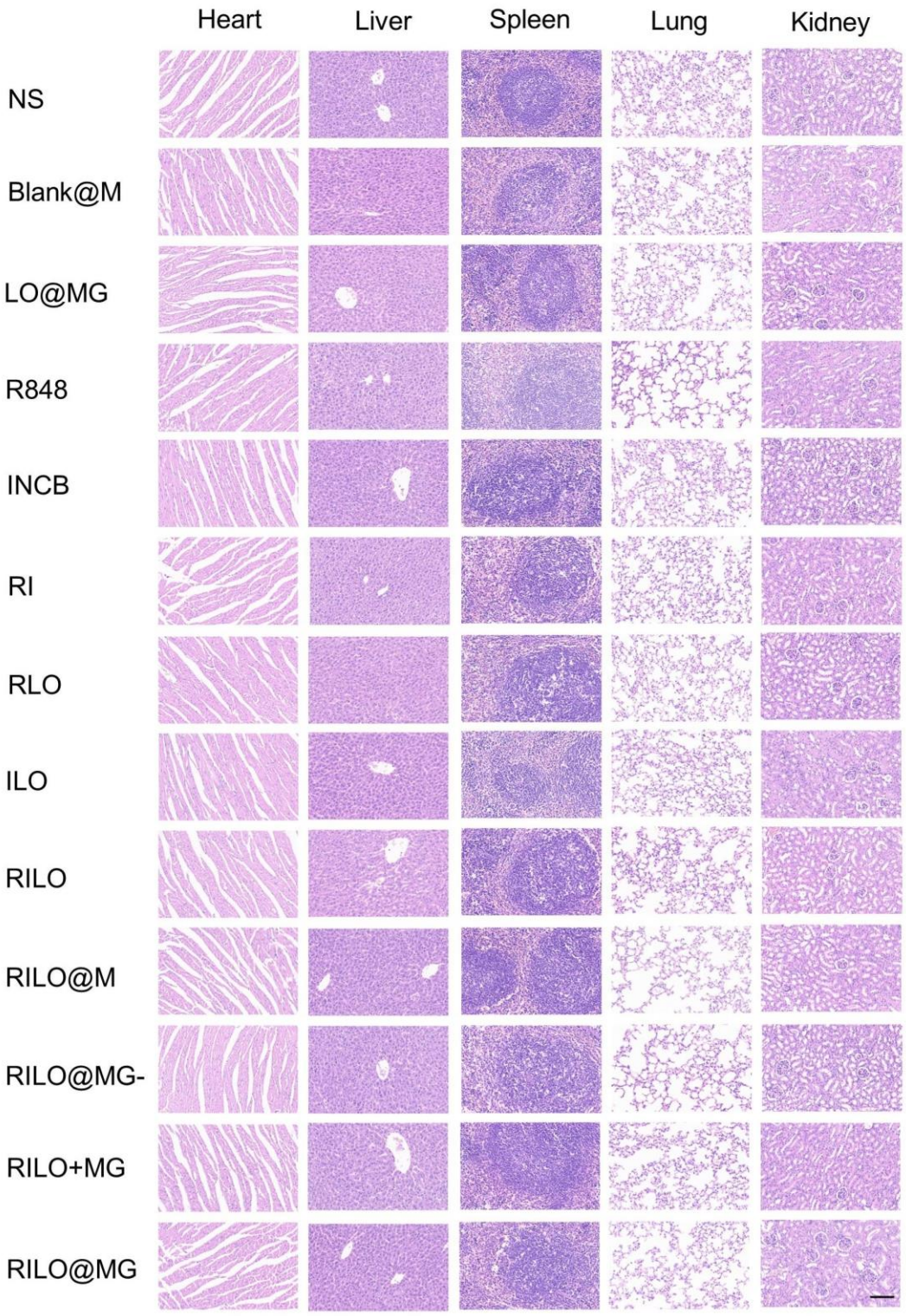

Supplementary Fig. 13. Representative images of major organs by microscopic pathological analysis related to Fig. 6a-f. Major organs were obtained at the study endpoint. H&E staining was performed on tissue sections for pathological assessment (*n* = 3 biologically independent experiments). Scale bar, 100 μm. No abnormal histological conditions (inflammation, necrosis, or structure changes) were reported and no differences between groups were observed.

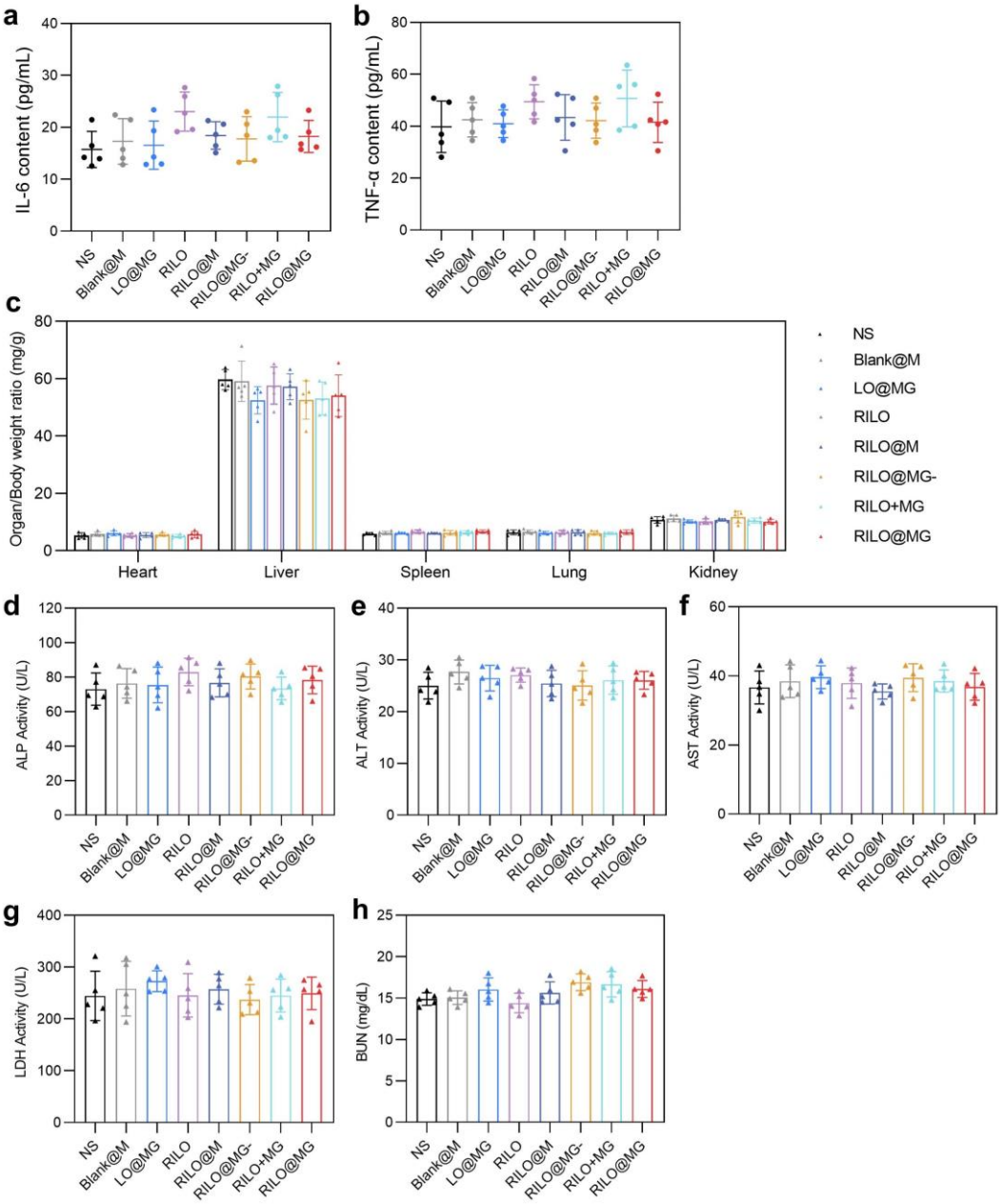

Supplementary Fig. 14. Preliminary safety evaluation of RILO@MG. a, b, Serum cytokine assessment after first i.v. administration. H22 tumour-bearing mice were i.v. administration at a dosage of 3.0 × 10^6 cells per mouse per injection, equal to 4 mg/kg R848 and 3.4 mg/kg INCB. Mice requiring injected formulations made by M1-type macrophages each received the equivalent number of cells (3.0 × 10^6 cells per mouse). Mice requiring injected other formulations each received the equivalent dose of medicine (4 mg/kg R848 and 3.4 mg/kg INCB). Serum cytokine concentrations including IL-6 (**a**) and TNF-α (**b**) were assessed at 48 h after the first injection. **c,** Organ/body weight ratio at the study endpoint related to Fig. 6a-f. Major organs were obtained at the study endpoint. **d-h,** Safety evaluation by liver and kidney function test related to Fig. 6a-f. Liver function indices including ALP (**d**), ALT (**e**), AST (**f**) and LDH (**g**), and kidney function index BUN (**h**) were assayed at the study endpoint. All data are shown as the mean ± SD with *n* = 5 biologically independent animals.

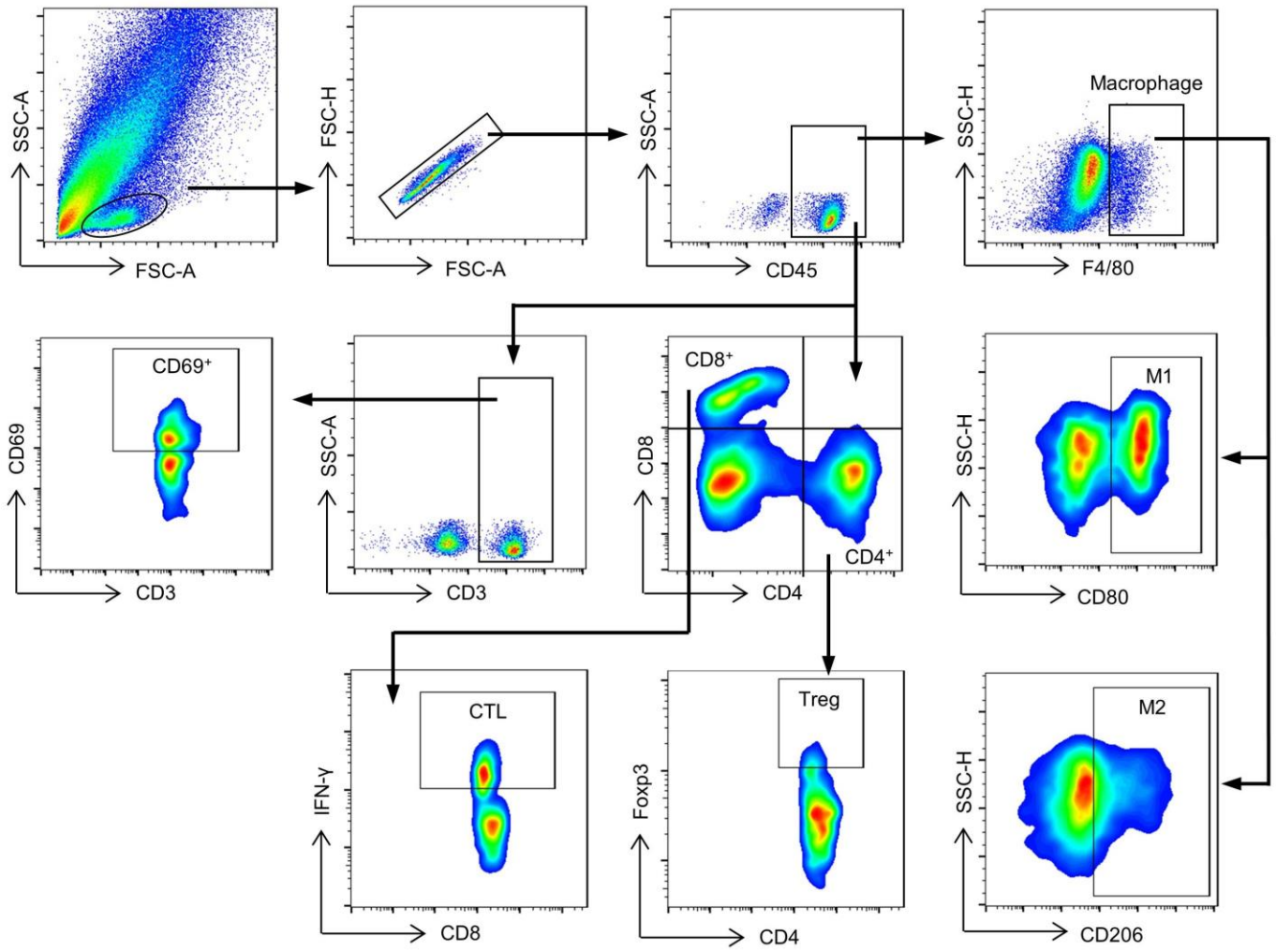

Supplementary Fig. 15. Flow cytometry gating strategy for analysis of intratumoural immune cells. Gating strategy for identifying $CD4^+$ T ($CD45^+CD4^+$) cells, $CD8^+$ T ($CD45^+CD8^+$) cells, $CD69^+$ T ($CD45^+CD3^+CD69^+$) cells, CTL ($CD45^+CD8^+IFN\text{-}\gamma^+$), Treg ($CD45^+CD4^+Foxp3^+$), M1-type macrophage ($CD45^+F4/80^+CD80^+$) and M2-type macrophage ($CD45^+F4/80^+CD206^+$) in the TME presented on Fig. 7c-i, Fig. 8e-h, Fig. 8l-o.

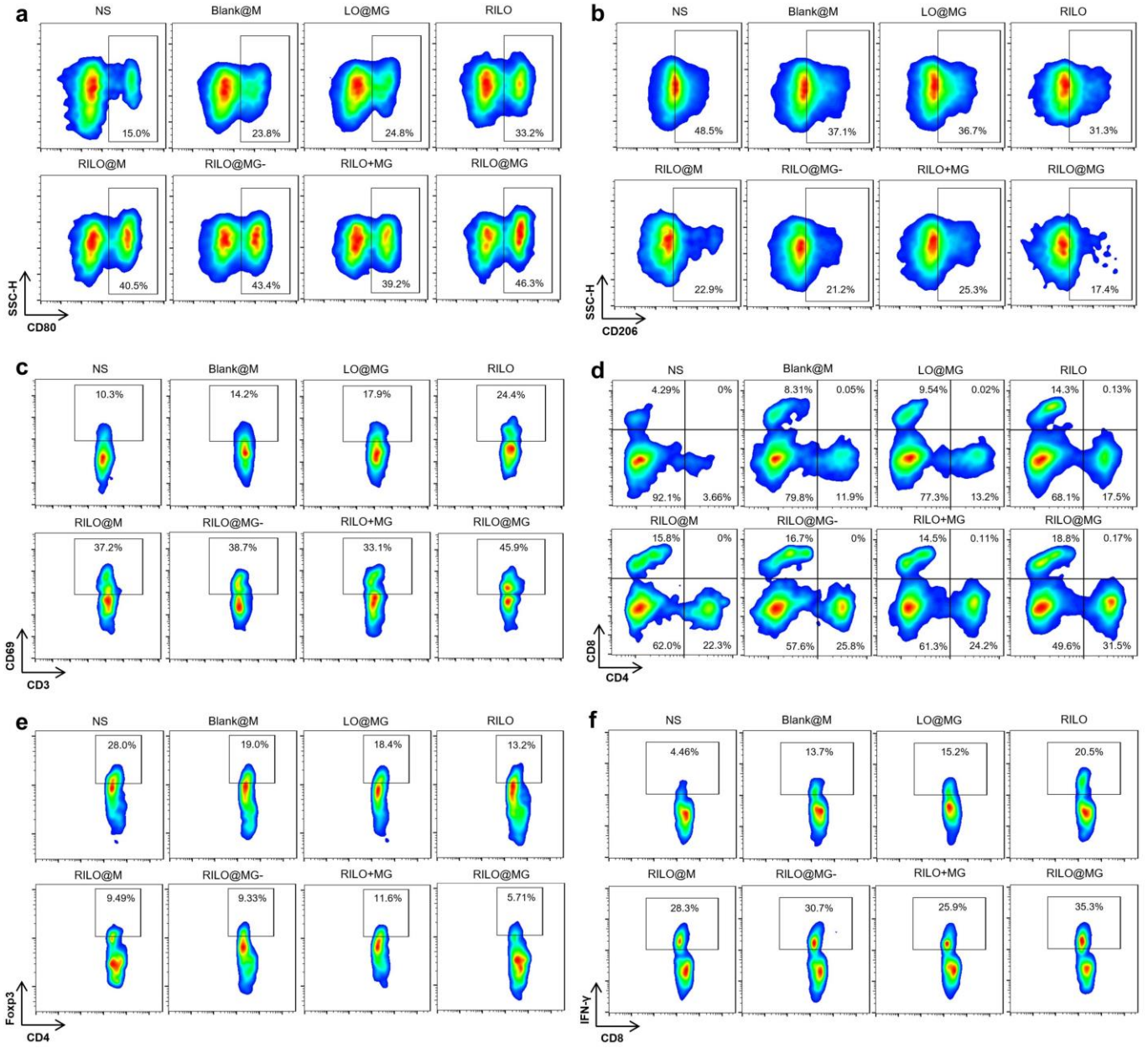

Supplementary Fig. 16. Representative flow cytometry plots related to Fig. 7c-i. Representative flow cytometry plots of intratumoural M1-type macrophage (**a**), M2-type macrophage (**b**), $CD69^+$ T cells (**c**), $CD4^+$ T cells (**d**), $CD8^+$ T cells (**d**), $CD4^+Foxp3^+$ T cells (**e**) and $CD8^+IFN\text{-}\gamma^+$ T cells (**f**).

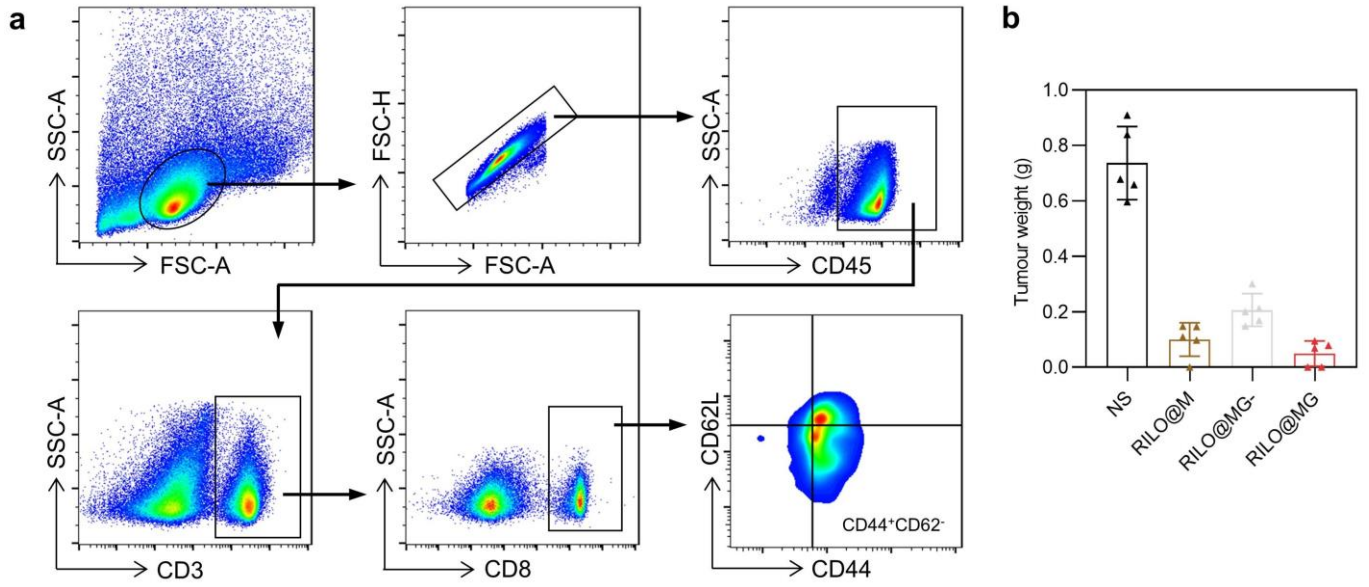

Supplementary Fig. 17. The evaluation of effector memory cells and memory immune responses. a, Gating strategy for identifying effector memory ($CD44^+CD62L^-$) $CD8^+$ T cells in spleens related to Fig. 7j. **b,** Tumour weights of re-challenged tumour related to Fig. 7k-m. All data are shown as the mean ± SD with *n* = 5 biologically independent animals.

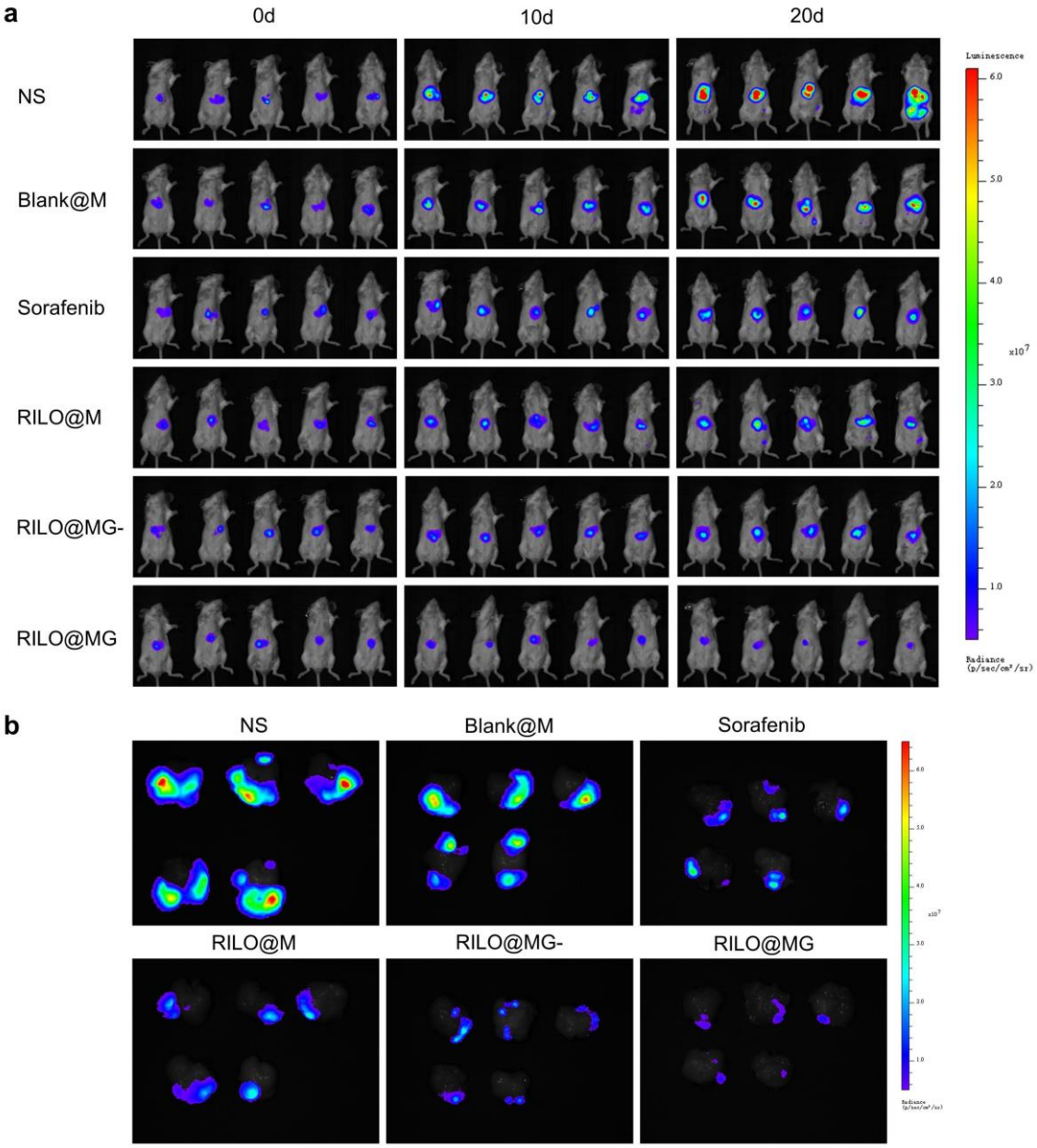

Supplementary Fig. 18. Efficacy validation in the orthotopic H22 tumour model related to Fig. 8a. a, In vivo bioluminescence images of orthotopic H22 tumour model related to Fig. 8a (*n* = 5 biologically independent animals). **b,** Ex vivo images of livers in the orthotopic H22 tumour model on Day 20 related to Fig. 8a (*n* = 5 biologically independent animals).

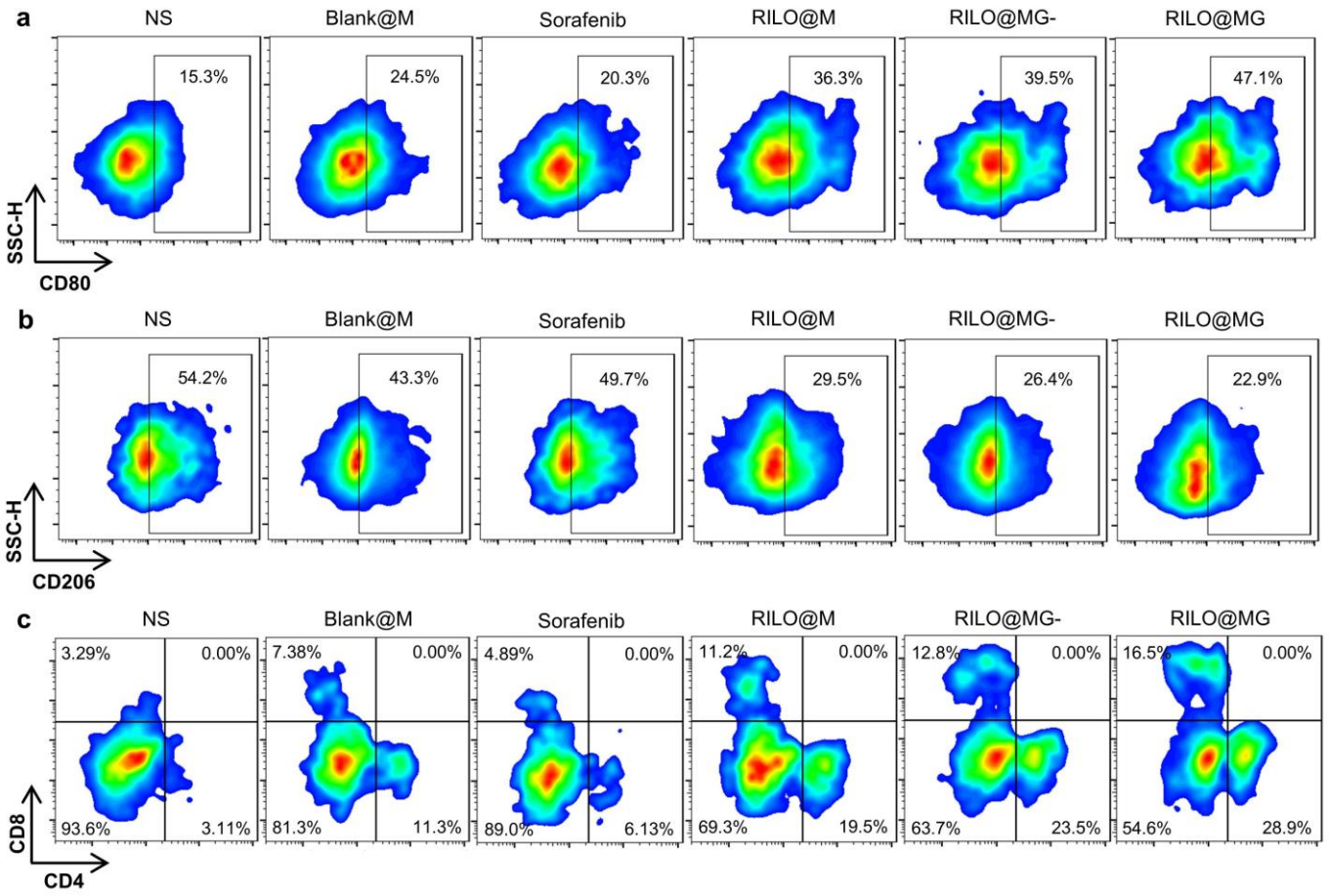

Supplementary Fig. 19. Flow cytometry data in the orthotopic H22 tumour model on Day 20 related to Fig. 8a. Representative flow cytometry plots of M1-type macrophage (**a**), M2-type macrophage (**b**), $CD4^+$ and $CD8^+$ T cells (**c**) in tumours of mice sacrificed on Day 20.

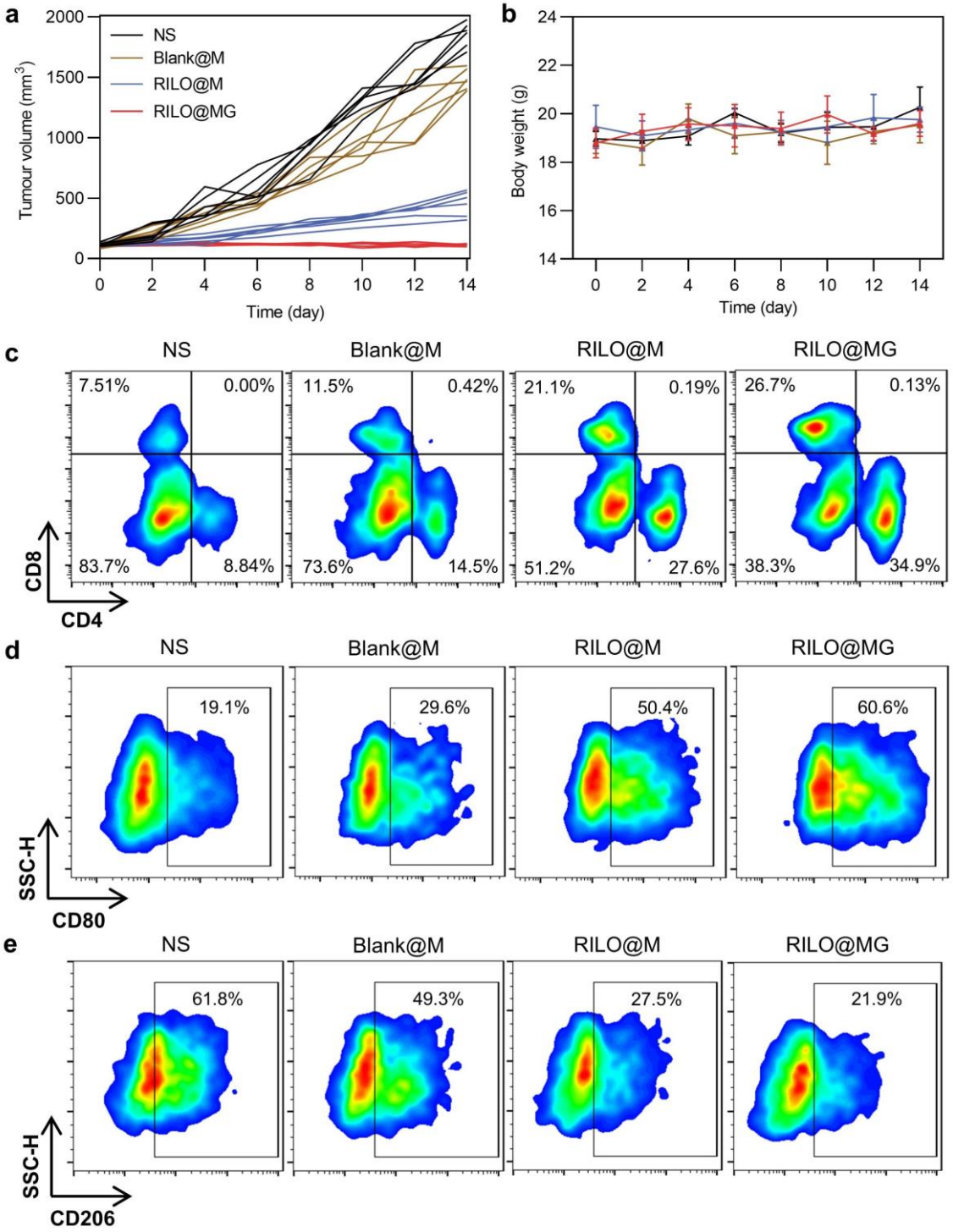

Supplementary Fig. 20. Tumour growth curves, body weight changes and flow cytometry data in the B16F10 tumour-bearing mouse model over the course of treatment related to Fig. 8i-o. a-b, Tumour growth curves (**a**) and body weight changes (**b**) of tumour-bearing mice were monitored over time (*n* = 6 biologically independent animals). **c-e,** Representative flow cytometry plots of $CD4^+$ and $CD8^+$ T cells (**c**), M1-type macrophage (**d**) and M2-type macrophage (**e**) in tumours of mice sacrificed. All data are shown as the mean ± SD.

Supplementary Table 1. Characterization of RIL, OMV and RILO. All data are shown as the mean ± SD with *n* = 3 biologically independent experiments.

	Size (nm)	PDI	Zeta potential (mV)	DL of R848(%)	EE of R848(%)	DL of INCB(%)	EE of INCB(%)
RIL	41.373±0.888	0.175±0.003	-2.528±0.285	6.314±0.103	96.529±1.739	6.469±0.046	98.900±0.862
OMV	39.627±1.732	0.248±0.036	-11.967±0.404	—	—	—	—
RILO	50.541±0.404	0.137±0.028	-7.443±0.308	6.167±0.022	97.659±0.244	5.134±0.145	81.303±2.413

DL, drug loading; EE, encapsulation efficiency.

Supplementary Table 2. Proteins identified from *E. coli* MG1655-origined OMV.

Index	Accession	Description	Molecular Weight (kDa)	Localization	Unique Peptides	Score
1	A0A484YCL0	60 kDa chaperonin	32.9	cytoplasm	4	182.34
2	A0A7H5D8I1	Major outer membrane lipoprotein Lpp	8.2	secreted	2	148.77
3	A0A6M0PGA3	60 kDa chaperonin	57.1	——	2	105.28
4	A0A377E6N8	Peptidoglycan-associated protein	16.8	outer membrane	3	90.67
5	A0A377D7F4	Outer membrane protein W	16.2	secreted	3	88.75
6	A0A7B1D042	Tol-Pal system protein TolB	45.9	——	6	88.47
7	D3H492	Pyruvate dehydrogenase E1 component	99.6	cytoplasm	12	87.5
8	A0A376MKW3	30S ribosomal protein S3	38.5	cytoplasm	6	87.19
9	A0A7L5L019	Scaffolding protein MipA	27.8	——	4	84.72
10	A0A2T1LF33	50S ribosomal protein L13	16	cytoplasm	3	81.99
11	A0A3L5QC40	50S ribosomal protein L10	17.7	——	4	78.14
12	A0A4S1UEN8	Outer membrane protein X	18.6	outer membrane	8	75.01
13	A0A2H9EUL1	Acetyltransferase component of pyruvate dehydrogenase complex	65.9	periplasm	10	51.74
14	A0A5B9AL25	Nucleoside-specific channel-forming protein Tsx	33.5	outer membrane	4	50.86
15	A0A077K781	30S ribosomal protein S13	13.1	cytoplasm	3	45.4
16	A0A7B7E5I8	Pectinesterase	46	——	4	44.23
17	A0A790ETA7	30S ribosomal protein S2	26.7	——	6	36.78
18	A0A7X1MK38	Dihydrolipoyl dehydrogenase	50.7	——	6	34.67
19	F4NDT5	Outer membrane protein N	40.4	outer membrane	6	33.5
20	A0A7L7M1X0	30S ribosomal protein S18	9	——	2	32.46
21	A0A6N7NKH4	Flagellin	29.6	——	4	31.55
22	A0A5N3D5X6	Class I fructose-bisphosphate aldolase	38.1	secreted	3	28.14
23	A0A6D0BSJ5	Penicillin-binding protein activator LpoA	72.8	secreted	5	27.88
24	F4NR29	Vitamin B12 transporter BtuB	70.1	outer membrane	6	26.3
25	A0A3W3FCN8	Lysine decarboxylase CadA	81.3	——	4	25.49

26	A0A6N7NB27	Uncharacterized protein	8.8	——	3	25.38
27	A0A7A5XKP8	Phospholipase A1	33.2	——	2	24.67
28	A0A781I9J6	Ferritin	19.4	——	2	24.26
29	A0A2X5PTL6	Catalase-peroxidase	80	cytoplasm	7	22.89
30	A0A6N7NE99	OmpA family protein	37	——	2	21.84
31	A0A192ETE7	Outer membrane channel protein TolC	53.7	——	4	21.57
32	A0A7U6ALM1	Aspartate ammonia-lyase	52.3	——	7	18.76
33	A0A376PV44	Phage major head protein (Major coat protein)	38	secreted	2	18.11
34	A0A776VE75	Omptin family outer membrane protease OmpT (Fragment)	21	——	4	17.95
35	A0A798ME49	30S ribosomal protein S20	9.7	——	2	17.91
36	D3QUE6	Acid stress chaperone HdeB	12.5	——	2	17.04
37	V0X8C4	30S ribosomal protein S9	9.7	cytoplasm	2	16.46
38	A0A3Y1JDX7	Maltose operon protein MalM	32	——	2	16.45
39	A0A377N362	FimH protein	31.4	fimbrium	3	15.76
40	A0A0K4G3J8	50S ribosomal protein L7/L12	12.3	periplasm	3	14.36
41	A0A7D7E3Q2	Peptidyl-prolyl cis-trans isomerase	28.9	——	3	13.92
42	A0A782HTS0	Formate C-acetyltransferase	85.3	——	3	12.84
43	F4NKN4	Inorganic pyrophosphatase	19.7	cytoplasm	4	12.65
44	A0A5E9Z9X9	Uridine phosphorylase	27.3	cytoplasm	3	11.92
45	A0A377BAB4	50S ribosomal protein L20	9.3	secreted	2	10.59
46	A0A785J6P1	Lysine--tRNA ligase	57.8	——	2	10.49
47	A0A7D7DZR1	Outer membrane protein assembly factor BamA	90.6	outer membrane	4	10.3
48	D6I8V0	Predicted protein	36.8	secreted	2	9.81
49	A0A376MMR1	Glutamine synthetase	43.7	cytoplasm	3	9.78
50	A0A376VBV1	Bacterioferritin	18.4	cytoplasm	2	9.21
51	A0A377DBF7	Bacterioferritin	18.3	cytoplasm	3	8.66
52	A0A7H9QT58	DUF883 domain-containing protein	11	inner membrane	2	7.94
53	A0A7T8PU92	Pyruvate kinase PykF	50.7	——	4	7.27

54	A0A782LSB2	Glutamine ABC transporter substrate-binding protein GlnH	27.2	——	2	6.84
55	A0A2A2CDP9	Putrescine-binding periplasmic protein	38.9	periplasm	2	6.63
56	A0A243UWG9	Thiol:disulfide interchange protein DsbA (Fragment)	22.2	——	3	6.62
57	A0A4T5REM4	6-phosphogluconate dehydrogenase, decarboxylating	51.4	secreted	2	6.46
58	A0A774CSQ3	Uncharacterized protein	11.4	——	2	6.33
59	A0A7Z6SEK6	Elongation factor Tu (Fragment)	35.4	——	2	6.2
60	A0A786ZMQ2	50S ribosomal protein L1	24.7	——	2	6.09
61	A0A7D7H5M8	Purine nucleoside phosphorylase DeoD-type	26	cytoplasm	2	5.99
62	A0A7B4KCG4	Chaperone protein DnaK	69.1	——	2	5.92
63	A0A271UAW6	Catabolite activator protein	23.6	——	2	5.87
64	A0A4Z0TLW4	Murein hydrolase activator NlpD	40.1	secreted	2	5.55
65	A0A6G6L5Y7	DNA protection during starvation protein	18.7	——	3	4.81
66	W1X2L6	DNA-directed RNA polymerase subunit (Fragment)	133.9	cytoplasm	2	4.65
67	A0A6N7NPD3	Catalase	78.1	——	2	3.79
68	A0A377CUE3	Ribonucleoside-diphosphate reductase	85.7	secreted	2	3.59
69	A0A2X1K7V0	Glyceraldehyde 3-phosphate dehydrogenase A	15.3	cytoplasm	2	3.03
70	C3TPA2	Lipoprotein	29.4	secreted	2	2.43
71	A0A7B9W8N5	Glutamine--tRNA ligase	63.5	——	2	1.76

Supplementary Table 3. Characterization of exosomes from Blank@M and RI-exosomes from RILO@MG- and RILO@MG. All data are shown as the mean ± SD with *n* = 3 biologically independent experiments.

	Size (nm)	Zeta potential (mV)
Blank@M	76.587±4.750	-10.233±0.208
RILO@MG-	89.357±4.106	-8.550±0.295
RILO@MG	87.573±4.208	-8.770±0.276